The Effects of Hydrophobic and Hydrophilic Graphene Nanoflakes on Methane Hydrate Kinetics

*Adam McElligott, Hasan Uddin, Jean-Luc Meunier, Phillip Servio**

Department of Chemical Engineering, McGill University, Montreal, Quebec H3A 0C5, Canada

ABSTRACT

Gas hydrate technologies have steadily gained interest in several industries for their potential use in natural gas transport and carbon dioxide sequestration applications. To further develop these emerging technologies, significant focus has been placed on additives, and particularly nanoparticles, which optimize their efficiencies. The addition of materials such as graphene nanoflakes (GNFs) has previously been proven to enhance the production of methane hydrates and other hydrate systems. In this study, the growth rates of methane hydrates were measured in the presence of both hydrophobic (as-produced) and hydrophilic (plasma-functionalized) GNFs at 2 °C and 4646 kPa. The effect of GNF loading in the aqueous phase for both types was also determined. Small-scale agglomeration limited the growth rate enhancement effect of hydrophobic GNFs at low concentrations of around 0.5 ppm while significantly increasing the formation kinetics by about 101% at concentrations of 5 ppm. At even higher concentrations (10 ppm), the performance decreased due to large-scale agglomeration. Enhancement rose rapidly at low

concentrations (0.1 to 1 ppm) of hydrophilic GNFs, peaking at about 288% before dropping to around 215% at 5 ppm due to mean free path limitations then rising again as surface area increased.

INTRODUCTION

Gas hydrates are non-stoichiometric crystalline compounds which form when either a gas or a volatile liquid occupies cavities formed by a network of hydrogen-bonded water molecules. The enclosed guest molecule must have the correct size to stabilize the host lattice through weak van der Waals forces[1]. First discovered in 1810 by Sir Humphrey Davy, research into gas hydrates, also called clathrate hydrates, was seen as a purely academic pursuit[2]. Hydrates only became relevant in industry in the 1930s when it was discovered that they form and block oil and gas pipelines[3]. Therefore, much research since has been focused on the inhibition of gas hydrate formation[4-6]. However, hydrates are now being used in a variety of technologies such as carbon dioxide sequestration, natural gas transport and storage, novel separation techniques, and refrigeration processes[1, 7-15]. It is therefore of great interest to study compounds that assist in the formation of hydrate structures as they can potentially be used to improve and further develop these technologies.

There are many groups of promoters which assist in the formation of gas hydrates. Among them, the two most commonly investigated are surfactants and nanoparticles. The promotion effects of these compounds can be thermodynamic, shifting the three-phase equilibrium curve to conditions more favourable to formation, or kinetic, inducing nucleation of stable gas hydrate crystals[16]. Recently, this class of promoters has been expanded to include materials such as graphene nanosheets or graphene nanoflakes (GNFs). These GNFs have been proven to increase the yields of several different gas hydrate compounds, including methane hydrates[17-22]. For example, Ghozatloo et al. (2015) found that the presence of Hummers' graphene increased methane storage

by 12.9 % compared to water[17] and Hosseini et al. (2015) found a 7.6 % methane storage increase in the presence of CVD graphene compared to a water/SDS system[21]. Rezaei et al. (2016) found that the presence of graphene oxide also increased ethylene storage in the hydrate phase compared to water[19].

GNFs are naturally hydrophobic and therefore adding them to an aqueous system can prove to be problematic as they can agglomerate and settle out of solution[23]. Solutions to this problem have included the addition of surfactants or chemical treatments to improve stability[20]. However, recent advancements allow for the functionalization of the GNF surface with oxygen-containing groups through a plasma decomposition process, resulting in a stable nanofluid[23]. Through covalent bonding with oxygenated functionalities such as carboxyl, hydroxyl and ether oxide groups, the aqueous GNFs have been shown to maintain their dispersion for at least six weeks[23]. This work focusses on evaluating the effects of functionalized GNFs on methane hydrate formation, which to the best of our knowledge has never been investigated.

The three steps to the formation of hydrates are saturation, induction, and growth[1]. These can be seen in Figure 1 below in the context of a gas consumption curve.

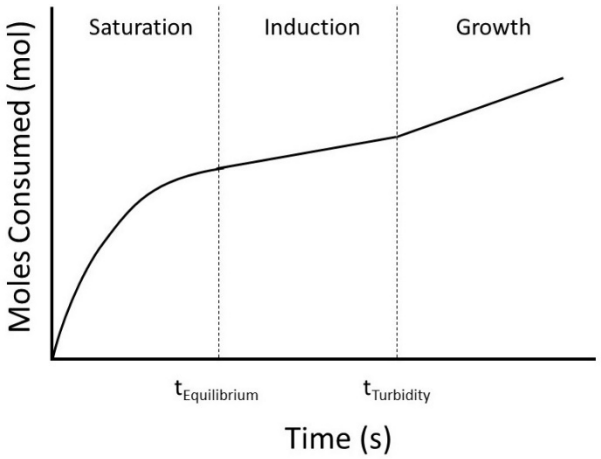

Figure 1. Three Phases of Hydrate Formation Seen Through a Gas Consumption Curve

The saturation step involves the inclusion molecule dissolving into the aqueous solution until the moles consumed reach the equilibrium concentration. This occurs at $t_{Equilibrium}$, which is the time when the solution becomes saturated. As more molecules continue to dissolve beyond this point, the solution becomes supersaturated; a regime in which hydrates can form[1]. This point is also where the induction phase begins. In this phase, whose length is considered a stochastic phenomenon, small hydrate crystals called nuclei form and dissociate continually until they attain a critical size[1]. At this point, marked as $t_{Turbidity}$ in the figure, the nucleus is energetically stable and autocatalytic growth of hydrate crystals may begin[1]. The range for the size of the critical nucleus is from 30 to 170 Å for methane hydrates[24]. The third phase, growth, is marked by an initial linear increase in inclusion body consumption with time and, for the analysis of growth kinetics, this region is that of interest. It is also important to note that hydrate growth is an exothermic process and a system's ability to dissipate heat can impact the growth rate significantly.

The aim of this study is to investigate the growth rates of methane hydrates in the presence of hydrophobic (as-produced) and hydrophilic (plasma-functionalized) GNFs at various concentrations. In previous studies, the total uptake of hydrate-forming gases after many hours of growth was measured, as well as induction time and the extent of hydrate dissociation. However, the kinetic growth rate evolution with loading of a well-dispersed nanomaterial such as GNF has never been studied up to now[17-22]. Furthermore, the concept of utilizing plasma-functionalized GNFs in gas hydrate systems is, to the best of our knowledge, entirely novel.

MATERIALS AND METHODS

Experiments were carried out in a crystallizer made from stainless steel 316. It is custom-built, with an internal diameter of 7.62 cm and walls 4.45 cm thick. The unit is designed to withstand up to 20 MPa of pressure. The chamber, which contains two polycarbonate windows for visual

observation of hydrates, has a 610 mL capacity. Liquid solutions are injected through a 0.32 cm NPT sample port. General-purpose platinum resistance temperature detectors (Omega RTDs, with a Class A accuracy of +/- 0.154 °C at experimental conditions) are used to monitor both liquid and gas phase temperatures. A Rosemount 3051 Smart Pressure Transmitter is used to monitor crystallizer pressure. The operating range of these transducers is 0-13780 kPa with an accuracy of 0.04% of the span. There is a 5.08 cm long magnetic stir bar at the base of the crystallizer to avoid mass transfer limitations. It is spun with a 1/8 HP, 90 V DC, 1750 RPM Leeson Electric Motor attached to a Neodymium External Horseshoe magnet. During hydrate formation, motor speed is set to 30% of maximum or 525 RPM. A schematic of the experimental apparatus can be seen in Figure 2 below.

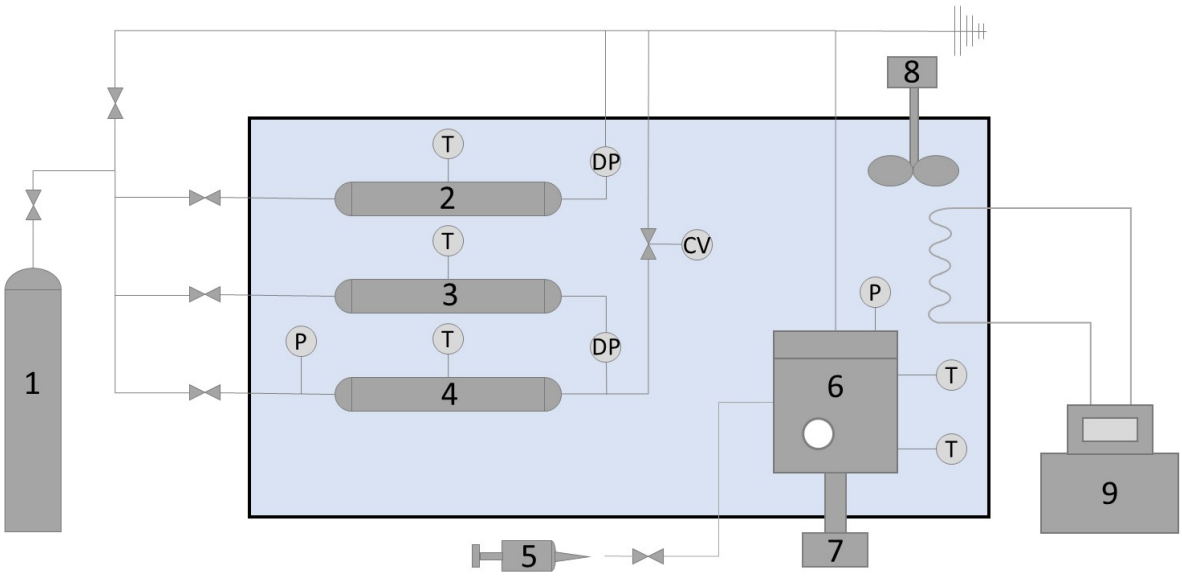

Figure 2. Experimental Apparatus Schematic (Simplified). Includes methane cylinder (1), reactor bias (2), reservoir bias (3), reservoir (4), sample injection (5), crystallizer (6), magnetic stirrer (7), electric stirrer (8) and chiller (9). T and P represent temperature and absolute pressure respectively, DP represents differential pressure and CV represents the control valve.

The crystallizer is submerged in a bath with a 50/50 volume mixture of water and ethylene glycol to control the system temperature. The bath temperature is controlled by a Neslab RTE 740 chiller, which also uses a 50/50 volume mixture of water and ethylene glycol as its cooling fluid. It can operate in the range of -40 to 200 °C. Temperature measurement accuracy is 0.01 °C. A Leeson Direct Current Permanent Magnet Motor is used to mix the bath fluid and maintain homogenous thermal conditions inside the bath.

The gas reservoir tank, also placed in the cooling bath, is used to maintain isobaric conditions in the crystallizer during the experiment. Gas from the reservoir is supplied via a Baumann 51000 Low Flow control valve. Reservoir gas temperature is measured by an RTD, and absolute reservoir pressure is monitored with a pressure transducer of the same type and model as found in the crystallizer. Also submerged are bias tanks for both the reservoir and crystallizer whose respective temperatures are measured via RTDs. Rosemount 3051 Smart Pressure Transmitters (operating range of 0-2000 kPa and accuracy of 0.04% of the span) are used to read differential pressure between the reactor and its bias as well as the reservoir and its bias. The reservoir differential is used to accurately measure the consumption of gas. The reactor differential is used to instruct control valve operation.

The methane used in the experiments is purchased from MEGS and is of Ultra High Purity. Oxygen-functionalized GNFs (O-GNFs) are produced in a two-stage process. The GNFs are produced first through a homogeneous nucleation process in which critical carbon clusters are formed from carbon vapours, typically in a temperature window between 4000-5000 K. Control of the temperature, flow, and nucleation fields allows for the 2-dimensional-only growth of these clusters and a pure powder of graphene sheets is formed. The bulk of this powder is deposited on a collecting plate inside the thermal plasma reactor. In the second stage of the process, the

methane/nitrogen gas feed is changed to air, the oxygen of which forms an active species that interacts with the GNF surface, producing hydrophilic groups of tunable quantity[23]. Both hydrophobic and hydrophilic particles are between 5 and 20 atomic layers thick (10 on average) and have in-plane dimensions roughly of 100 x 100 nm. X-ray photoelectron spectroscopy (XPS) on the O-GNF and nanofluid stability tests indicate that reaching an atomic composition of approximately 14.2% oxygen provides a stable nanofluid with no agglomeration over periods of several weeks to months[23]. Deconvolution of the oxygen and carbon XPS peaks indicated the presence of C-O, C=O and O=C-O bonds, which can correspond to hydrophilic groups such as esters, carboxylic groups, anhydrides, hydroxyls and ether oxides[23]. Hydrophilic GNFs were shown to become perfectly dispersed in water without surfactant, while hydrophobic GNFs do not mix in the presence of water[23]. Hydrophobic GNF solutions were therefore mixed through ultrasonication with a Hielscher UP200S ultrasonic processor (cycling at 0.5 and 50% max amplitude) while hydrophilic ones were mixed by a magnetic stir bar on a magnetic stir plate. Further information regarding production, functionalization, characterization and imaging of the GNFs used in this study can be found in Legrand et al. (2016).

The crystallizer was cleaned five times with 360 mL of RO water (0.22 μm filter, conductivity of 10 μS, total organic content of less than 10 ppb) before any liquid sample was injected. The experimental solution was then loaded into the crystallizer through the sample port. The solution was then cooled to the desired temperature by the Neslab RTE chiller, after which the crystallizer was pressurized with methane to the desired pressure. The control valve was set when the temperature and pressure reached steady state to maintain isobaric conditions and the stir bar was initiated. Data was obtained through a LabVIEW™ Virtual Instrument, and molar consumption values were obtained in MATLAB® by converting reservoir differential pressure into moles

through the Trebble-Bishnoi equation of state[25]. The linear region of the consumption curve, which begins with the formation of a critical nucleus, was used to determine the growth rate. Only the first 15 minutes of data after the turbidity point (one data point is generated every second) was used to calculate the rate of formation as viscosity changes as well as mass transfer resistance from hydrate formation are at a minimum in this timeframe and thus the methane consumption rate remains constant. Analysis was done by comparing the growth rates of GNF-containing solutions to a baseline of pure water.

Experiments were conducted at 2 °C and a pressure of 4646 kPa. This corresponds to a pressure driving force of 1500 kPa from the three-phase equilibrium curve[26] as can be seen in Figure 3. Hydrophobic (as-produced) and hydrophilic (plasma-functionalized) GNFs were each individually injected at concentrations of 0.1, 0.5, 1, 5 and 10 ppm. This corresponds to the same regime of experiments as Pasieka et al. (2013) which will also act as a point of comparison. GNF concentrations below 0.1 ppm were not feasible as instruments to generate such low concentration solutions reproducibly were not available. Each experiment consisted of five replicates, and RO water was used as the baseline for all GNF nanofluids and as a control.

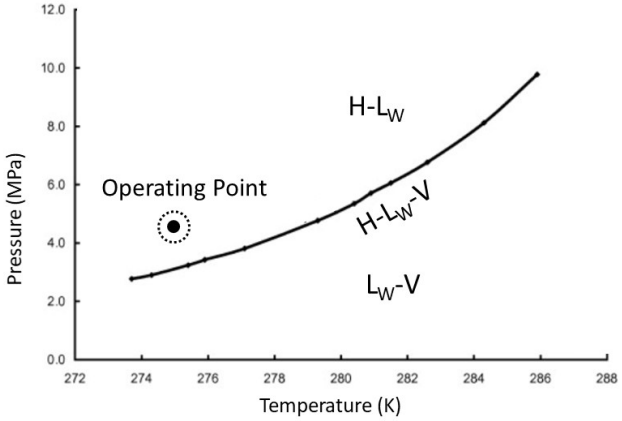

Figure 3. Methane Hydrate Equilibrium Curve Modified from Deaton et al. (1946)

RESULTS AND DISCUSSION

1. HYDROPHOBIC GNF EFFECTS

It was found that systems containing as-produced GNFs had enhanced methane hydrate growth rates compared to the water baseline. The rates of methane consumption for each GNF concentration in this series and their corresponding enhancement percentages can be found in Table 1 and Figure 4. In the presence of GNFs, growth rates increased by up to 101.38 % compared to the baseline. Hydrate promotion from graphene compounds has been seen in previous investigations[17-22]. However, these investigations were focused on the total uptake of gas after several hours, induction time and hydrate dissociation rather than the actual hydrate growth rate, particularly with loading[17-22]. Many of these studies propose that enhanced hydrate production occurs through three main phenomena. The first is that the nanofluid has a higher heat transfer coefficient which facilitates the system's heat dissipation. This results in a lower, more controlled temperature in the liquid and thus more stable hydrate production[17-22]. However, both experimental and modeling studies indicate limited to no heat transfer enhancement from nanofluids, but strong effects related to mass transfer enhancement in the fluid[27]. As discussed later, such enhancement of the transport of methane to potential hydrate sites could play an important role in hydrate production. The second involves the GNFs acting as sites for heterogeneous nucleation, which occurs on a pre-existing surface or interface. This type of nucleation requires less energy to form critical nuclei than bulk, or homogeneous, nucleation provided the surface has sufficient undercooling[28]. It is therefore proposed that the increased inhomogeneity of the solution caused by the presence of nanoparticles results in a large number of heterogeneous active sites such that many nanometric nuclei form and more gas is stored within water molecule cavities[17-22]. However, from both the above and our experiments, it is not clear whether the particles had sufficient undercooling for heterogeneous nucleation to occur. Instead, the particles may merely have been

pushed out of solution by the growing hydrate front, a phenomenon observed upon solidification of a water-based nanofluid to ice[29]. The third proposed phenomenon is an enhanced mass transfer rate from a high specific surface area to volume ratio and larger gas/liquid interfacial area[17-22]. Studies have reported an increase in gas/liquid interfacial area with the addition of nanoparticles and claim this to be the most substantial factor in determining mass transfer enhancement[30]. Several studies have also suggested that nanofluids have increased mass transfer coefficients compared to fluids not containing nanoparticles[30-32]. Nanoparticles have also been shown to aid mass transfer through the shuttle effect and hydrodynamic effects on the boundary layer between liquid and gas[33]. The shuttle effect occurs when gas molecules adsorb onto the nanoparticles surface, transporting additional gas to the liquid bulk and thus increasing the mass transfer coefficient[34]. The hydrodynamic effect occurs when nanoparticles collide and interact with the gas-liquid interface, increasing the mass transfer coefficient by thinning the effective diffusion layer[35].

Table 1. Methane Consumption Rates and Corresponding Enhancement for Different GNF Loadings

Loading (GNF ppm)	**Methane Consumption Rate (x10^{-5} mol s^{-1})**	**Enhancement (%)**	**95 % Confidence Interval (± %)**
0	1.18	0.00	2.94
0.1	1.86	58.42	5.82
0.5	1.90	61.96	6.37
1	1.82	54.82	5.04
5	2.37	101.38	7.61
10	1.98	68.63	3.58

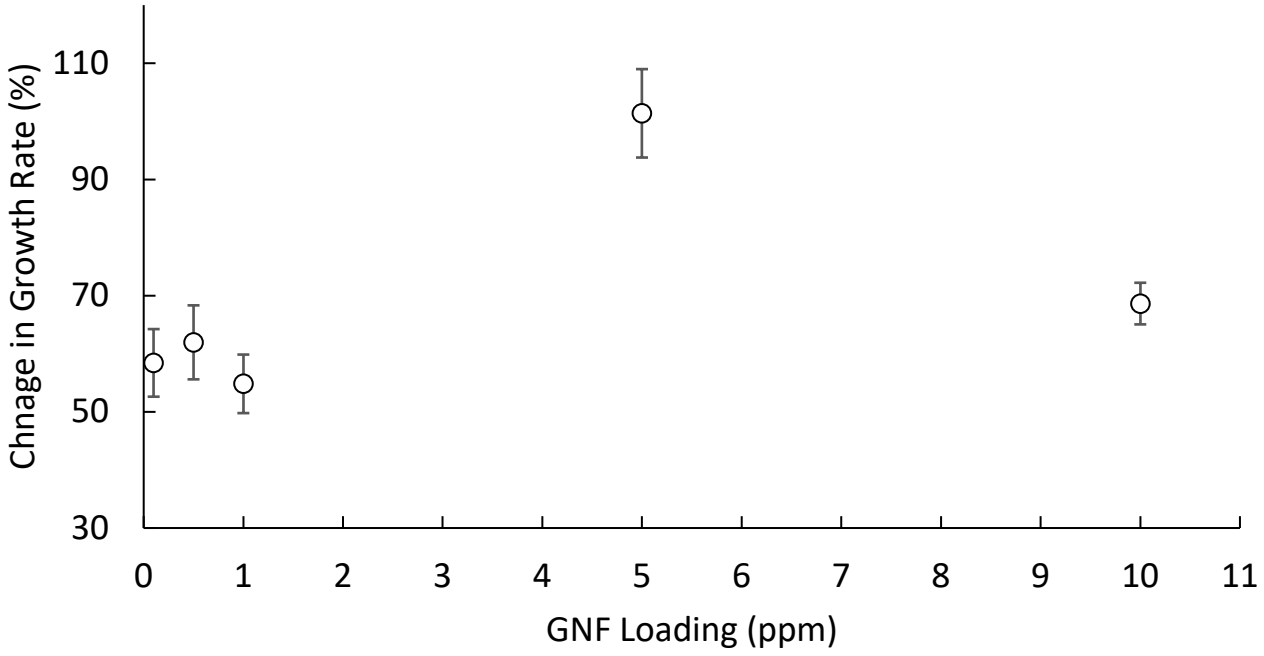

Figure 4. Methane Hydrate Growth Rate Enhancement versus As-Produced GNF Loading

2. HYDROPHOBIC GNF LOADING

Experiments were conducted at five different GNF concentrations which were then compared to a water baseline. A summary of these results can be found in Figure 4 and an outline of the proposed mechanism is found in Figure 5. Each point in Figure 4 is an average enhancement consisting of five replicates. The 95 % confidence interval is shown through the error bars. The hydrophobic GNF loading begins with an initial enhancement of 58.42 % at 0.1 ppm. As mentioned, experiments below this concentration could not be conducted as the masses required to create such solutions were not feasible to measure with an acceptable level of reproducibility. The consumption rate enhancement remained constant within error through the next two loadings before a significant increase at 5 ppm. In other words, the addition of nanoparticles before 5 ppm but after 0.1 ppm did not have a notable effect on the water-methane-hydrate system. It is expected that enhancement would increase with loading as total GNF surface area would also increase.

However, some small-scale agglomeration, which occurs in GNF nanofluids over time[23], may be occurring at these loadings. In fact, this agglomeration was observed visually upon sample removal for all loadings. This would limit the increase in surface area. Furthermore, aggregation of particles in nanofluids limits the effective mass transfer and thermal conductivity properties of the solution[36]. These together can result in a statistically constant enhancement.

The increase in enhancement at the loading of 5 ppm can be attributed to a greater available GNF surface area and thus a greater liquid/gas interfacial area. Methane is particularly likely to be found on the as-produced GNF surface as they are both hydrophobic. A larger surface area, therefore, allows more methane to be "shuttled" into the solution and become more available. This increase would be significant enough to overcome any minor agglomeration limitations occurring at lower loadings, resulting in a notable improvement in enhancement. The decrease in enhancement observed at 10 ppm can be due to predominant, large-scale agglomeration, which occurs commonly in higher-concentration GNF nanofluids over time[37]. At this concentration, the effect of GNF clustering would result in a reduction in available surface area and thus a reduction of the promotion of interfacial mass transfer. Additionally, Li et al. (2019) suggest that graphene aggregates may recruit methane molecules to adsorb onto their surfaces such that less methane is available to the system[38].

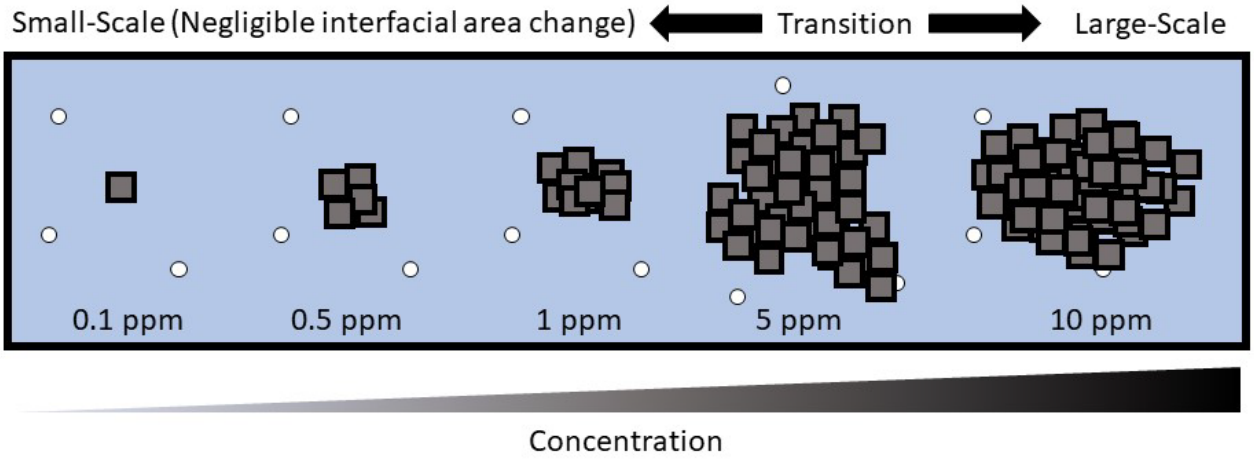

Figure 5. Proposed Mechanism for Hydrophobic GNF Loading Effects

3. HYDROPHILIC GNF EFFECTS

It was found that systems containing plasma-functionalized GNFs (O-GNFs) had enhanced methane hydrate growth rates compared to the water baseline. The rates of methane consumption for each O-GNF concentration in this series and their corresponding enhancement percentages can be found in Table 2 and Figure 6. In the presence of O-GNFs, growth rates strongly increased by practically a factor of four (up to 287.99 %) compared to water without dispersed nanoparticles. This is significantly higher than those of the hydrophobic as-produced GNFs. This behaviour is likely the result of the oxygen functional groups which are present on the O-GNF surface and generating hydrophilic behavior with good and stable dispersion, contrary to the as-produced GNFs. This stability can assist with liquid phase mixing as well as improve mass transfer between unfilled water cages and methane gas molecules. Micro-convection currents created by nanoparticle motion (i.e. Brownian agitation) result in enhanced mass diffusivity at the macroscopic level[27, 39]. This agitation in a solution of well-dispersed nanoparticles results in greater mixing and thus improved mass transfer of dissolved methane gas[33]. The enhancement can also be accounted for with the aforementioned phenomena of higher heat and mass transfer

coefficients, heterogeneous nucleation and a larger gas/liquid interfacial area which occur in two-phase nanofluid systems[17-22, 30-32].

Table 2. Methane Consumption Rates and Corresponding Enhancement for Different O-GNF Loadings

Loading (O-GNF ppm)	**Methane Consumption Rate ($x10^{-5}$ mol s^{-1})**	**Enhancement (%)**	**95 % Confidence Interval (± %)**
0	1.18	0.00	2.94
0.1	2.68	128.20	6.17
0.5	3.57	203.78	9.87
1	4.56	287.99	13.93
5	3.70	214.96	5.82
10	4.08	246.95	16.40

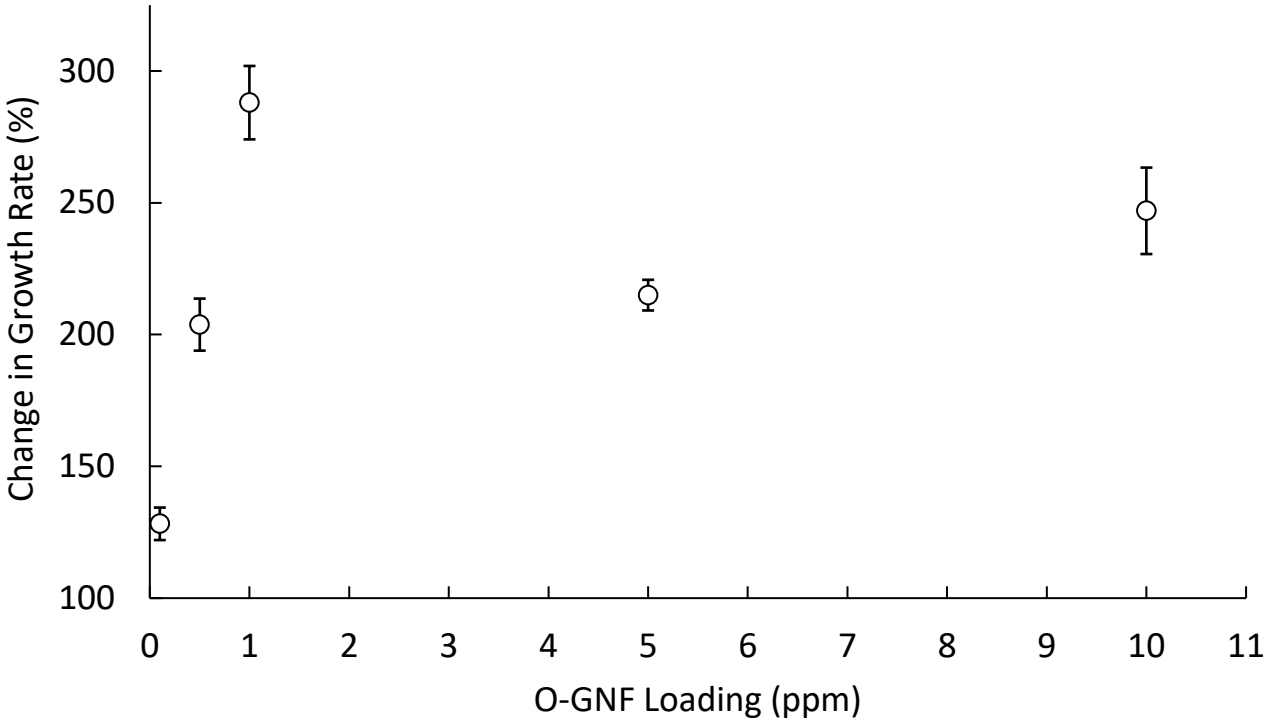

Figure 6. Methane Hydrate Growth Rate Enhancement versus Plasma-Functionalized GNF Loading (Water Excluded for Clarity)

4. Hydrophilic GNF Loading

The hydrophilic GNF experiments were conducted in the same way as for the hydrophobic GNFs. A summary of these results can be found in Figure 6 and an outline of the proposed mechanism is found in Figure 7. Over the concentration range, there are two distinct regimes. The first regime, from 0.1 to 1 ppm O-GNF, is a linear region where enhancement increases with loading. This is followed by a maximum at around 1 ppm after which there is a second regime from 5 to 10 ppm. This behaviour is similar to a study by Pasieka et al. (2013) who examined the effects of plasma-functionalized multi-walled carbon nanotubes (MWNTs) over the same concentration range for methane hydrate growth rates at the same temperature and pressure as in the current study. In that study, the two distinct regimes were also separated by a drop in

enhancement[40]. The nature of the two regimes, however, as well as the level of enhancement, are not the same. In the MWNT study, the maximum enhancement of about 16 % occurred at 0.1 ppm then decreased non-linearly until 1 ppm where a linear, increasing region developed[40]. It is likely that the difference in geometry and aspect ratio of the two nanoparticles accounts for the difference in behaviour as these can affect properties such as thermal conductivity, mass transfer, and nanofluid viscosity[41]. It is hypothesized that the GNFs can orient themselves more easily into depressions in the moving hydrate front, where MWNTs would be pushed out, further improving local heat transfer and mixing. Moreover, the structure of graphene is more conducive to heterogeneous nucleation[19].

The nature of the first regime is evidence that Brownian agitation is occurring in the nanofluid. The diffusivity of the gaseous solute on the solid nanoparticle phase is significantly lower than in the liquid phase. Therefore, mass diffusivity would decrease monotonically with loading if Brownian agitation were not occurring[27, 39]. Instead, one can assume mass transfer enhancement reaches a maximum followed by a dip which is potentially caused by the GNF mean free path, the distance between nanoparticle collisions, becoming too small. With an increase in the number of similar particles, the free motion of O-GNFs undergoing Brownian motion could face greater opposition. This would counteract improvements in mass diffusivity[39].

In the second regime, at loadings above 1 ppm, the enhancement which occurs can be attributed to a greater available GNF surface area. While it cannot be determined whether that region is linear, the rise in enhancement from the loadings of 5 to 10 ppm can also be ascribed to an increase in heterogeneous nucleation sites. Additionally, an increase in the number of dispersed GNFs may increase mass transfer across the gas/liquid interface. These loading effects differ significantly from those for the as-produced (hydrophobic) GNFs. The hydrophilic GNFs increased

enhancement with loading even at lower concentrations as agglomerates did not form at any scale. Additionally, there was no large-scale agglomeration at higher loadings because of better hydrophilic nanoparticle dispersion and thus there was an increase in enhancement rather than a reduction observed.

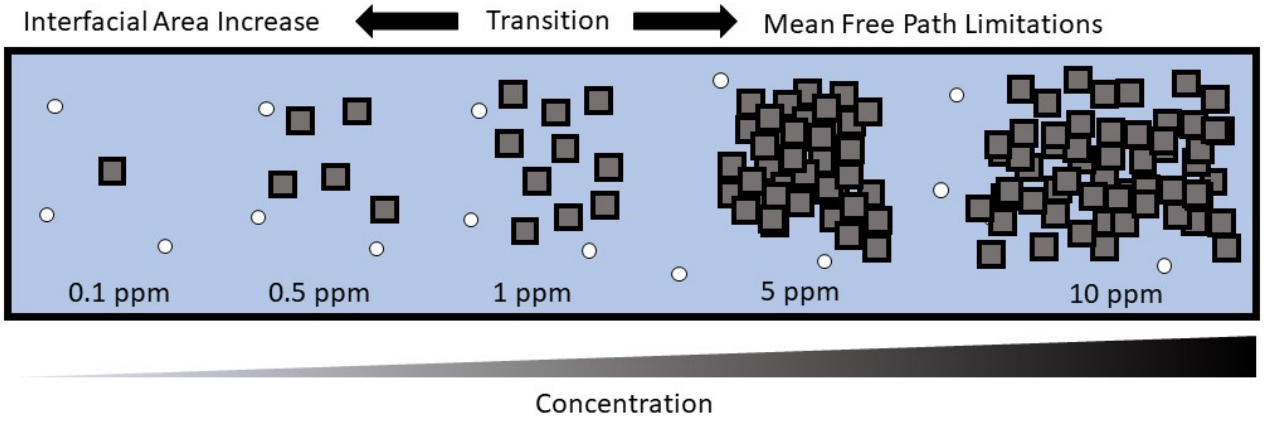

Figure 7. Proposed Mechanism for the Hydrophilic O-GNF Loading Effects

CONCLUSIONS

Hydrophobic (as-produced) and hydrophilic (plasma-functionalized) GNFs both enhance the growth rates of methane hydrates compared to water baselines. However, the extent of this enhancement and the effect of different loadings differ significantly between the GNF types. For the hydrophobic GNFs, after an initial rise to 58.42 % enhancement at 0.1 ppm, enhancement did not change until a loading of 5 ppm. This was attributed to small-scale agglomeration as hydrophobic nanoparticles tend to form clusters in solution. The rise to 101.38 % enhancement at 5 ppm was ascribed to an increase in liquid/gas interfacial area overcoming this agglomeration, while the drop in enhancement at the highest loading of 10 ppm was associated with potential large-scale agglomeration. For the hydrophilic GNFs, enhancement rose rapidly from 128.20 % at 0.1 ppm to a maximum of 287.99 % at 1 ppm. This significant increase was attributed to enhanced mass diffusivity caused by Brownian motion where micro-convection currents are created by GNF

motion. The enhancement dropped at 5 ppm concentrations of the hydrophilic nanoparticle due to mean free path limitations, a smaller distance between GNF collisions resulting from a higher concentration, hindering nanoparticle motion. At larger GNF loadings, the growth rate increased again simply due to an increase in available surface area for hydrate nucleation and gas/liquid interactions.

AUTHOR INFORMATION

Corresponding Author

*phillip.servio@mcgill.ca

Author Contributions

The manuscript was written through contributions of all authors. All authors have given approval to the final version of the manuscript.

ACKNOWLEDGEMENTS

The authors would like to acknowledge the financial support from the Natural Sciences and Engineering Research Council of Canada (NSERC). We would also like to acknowledge Faraz Rajput for his assistance with the setup and operation of the experimental apparatus.

REFERENCES

1. Sloan, E. D.; Koh, C. A., *Clathrate Hydrates of Natural Gases, Third Edition*. 3rd ed.; CRC Press: Boca Raton, Fl., 2008.

2. Davy, H., On some of the combinations of oxymuriatic gas and oxygene, and on the chemical relations of these principles, to inflammable bodies. *Philosophical Transactions of the Royal Society* **1811,** (101), 1-35.

3. Hammerschmidt, E. G., Formation of Gas Hydrates in Natural Gas Transmission Lines. *Industrial & Engineering Chemistry* **1934,** *26* (8), 851-855.

4. Heidaryan, E.; Salarabadi, A.; Moghadasi, J.; Dourbash, A., A new high performance gas hydrate inhibitor. *Journal of Natural Gas Chemistry* **2010,** *19* (3), 323-326.

5. Daraboina, N.; Pachitsas, S.; von Solms, N., Natural gas hydrate formation and inhibition in gas/crude oil/aqueous systems. *Fuel* **2015,** *148*, 186-190.

6. Zhukov, A. Y.; Stolov, M. A.; Varfolomeev, M. A., Use of Kinetic Inhibitors of Gas Hydrate Formation in Oil and Gas Production Processes: Current State and Prospects of Development. *Chemistry and Technology of Fuels and Oils* **2017,** *53* (3), 377-381.

7. Linga, P.; Kumar, R.; Englezos, P., The clathrate hydrate process for post and pre-combustion capture of carbon dioxide. *Journal of Hazardous Materials* **2007,** *149* (3), 625-629.

8. Ma, Z. W.; Zhang, P.; Bao, H. S.; Deng, S., Review of fundamental properties of CO2 hydrates and CO2 capture and separation using hydration method. *Renewable and Sustainable Energy Reviews* **2016,** *53*, 1273-1302.

9. Taylor, M.; Dawe, R. A.; Thomas, S., Fire and Ice: Gas Hydrate Transportation - A Possibility for the Caribbean Region. In *SPE Latin American and Caribbean Petroleum Engineering Conference*, Society of Petroleum Engineers: Port-of-Spain, Trinidad and Tobago, 2003.

10. Eslamimanesh, A.; Mohammadi, A. H.; Richon, D.; Naidoo, P.; Ramjugernath, D., Application of gas hydrate formation in separation processes: A review of experimental studies. *The Journal of Chemical Thermodynamics* **2012,** *46*, 62-71.

11. Babu, P.; Kumar, R.; Linga, P., Pre-combustion capture of carbon dioxide in a fixed bed reactor using the clathrate hydrate process. *Energy* **2013,** *50*, 364-373.

12. Chatti, I.; Delahaye, A.; Fournaison, L.; Petitet, J.-P., Benefits and drawbacks of clathrate hydrates: a review of their areas of interest. *Energy Conversion and Management* **2005,** *46* (9), 1333-1343.

13. Englezos, P., Extraction of methane hydrate energy by carbon dioxide injection-key challenges and a paradigm shift. *Chinese Journal of Chemical Engineering* **2019**.

14. Yan, J.; Lu, Y.-Y.; Zhong, D.-L.; Zou, Z.-L.; Li, J.-B., Enhanced methane recovery from low-concentration coalbed methane by gas hydrate formation in graphite nanofluids. *Energy* **2019,** *180*, 728-736.

15. Xia, Z.-M.; Li, X.-S.; Chen, Z.-Y.; Li, G.; Yan, K.-F.; Xu, C.-G.; Lv, Q.-N.; Cai, J., Hydrate-based CO2 capture and CH4 purification from simulated biogas with synergic additives based on gas solvent. *Applied Energy* **2016,** *162*, 1153-1159.

16. Kumar, A.; Bhattacharjee, G.; Kulkarni, B. D.; Kumar, R., Role of Surfactants in Promoting Gas Hydrate Formation. *Industrial & Engineering Chemistry Research* **2015,** *54* (49), 12217-12232.

17. Ghozatloo, A.; Hosseini, M.; Shariaty-Niassar, M., Improvement and enhancement of natural gas hydrate formation process by Hummers' graphene. *Journal of Natural Gas Science and Engineering* **2015,** *27*, 1229-1233.

18. Zhou, S.-d.; Yu, Y.-s.; Zhao, M.-m.; Wang, S.-l.; Zhang, G.-Z., Effect of Graphite Nanoparticles on Promoting CO2 Hydrate Formation. *Energy & Fuels* **2014,** *28* (7), 4694-4698.

19. Rezaei, E.; Manteghian, M.; Tamaddondar, M., Kinetic study of ethylene hydrate formation in presence of graphene oxide and sodium dodecyl sulfate. *Journal of Petroleum Science and Engineering* **2016,** *147*, 857-863.

20. Wang, F.; Meng, H.-L.; Guo, G.; Luo, S.-J.; Guo, R.-B., Methane Hydrate Formation Promoted by −SO3−-coated Graphene Oxide Nanosheets. *ACS Sustainable Chemistry & Engineering* **2017,** *5* (8), 6597-6604.

21. Hosseini, M.; Ghozatloo, A.; Shariaty-Niassar, M., Effect of CVD graphene on hydrate formation of natural gas. *Journal of Nanostructure in Chemistry* **2015,** *5* (2), 219-226.

22. Saeid Abedi-Farizhendi; Mina Iranshahi; Abolfazl Mohammadi; Mehrdad Manteghian; Amir H. Mohammadi, Kinetic study of methane hydrate formation in the presence of carbon nanostructures. *Petroleum Science* **2019,** (16), 657-668.

23. Legrand, U.; Mendoza Gonzalez, N. Y.; Pascone, P.; Meunier, J. L.; Berk, D., Synthesis and in-situ oxygen functionalization of deposited graphene nanoflakes for nanofluid generation. *Carbon* **2016,** *102*, 216-223.

24. Englezos, P.; Kalogerakis, N.; Dholabhai, P. D.; Bishnoi, P. R., Kinetics of formation of methane and ethane gas hydrates. *Chemical Engineering Science* **1987,** *42* (11), 2647-2658.

25. Trebble, M. A.; Bishnoi, P. R., Development of a new four-parameter cubic equation of state. *Fluid Phase Equilibria* **1987,** *35* (1), 1-18.

26. Deaton, W. M.; Frost, E. M., *Gas Hydrates and Their Relation to the Operation of Natural Gas Pipe Lines*. American Gas Association: 1946; Vol. 8, p 101.

27. Veilleux, J.; Coulombe, S., A dispersion model of enhanced mass diffusion in nanofluids. *Chemical Engineering Science* **2011,** *66* (11), 2377-2384.

28. Callister, W. D.; Rethwisch, D. G., *Materials Science and Engineering: An Introduction*. 8 ed.; John Wiley and Sons, Inc.: Hoboken, NJ, 2010.

29. Ivall, J.; Hachem, M.; Coulombe, S.; Servio, P., Behavior of Surface-Functionalized Multiwall Carbon Nanotube Nanofluids during Phase Change from Liquid Water to Solid Ice. *Crystal Growth and Design* **2015,** *15* (8), 3969-3982.

30. Bernat Olle; Seyda, B.; Tracy, C. H.; Lev, B.; T. Alan Hatton, a.; Daniel, I. C. W., Enhancement of Oxygen Mass Transfer Using Functionalized Magnetic Nanoparticles. **2006**.

31. Zhu, H.; Shanks, B. H.; Heindel, T. J., Enhancing CO−Water Mass Transfer by Functionalized MCM41 Nanoparticles. *Industrial & Engineering Chemistry Research* **2008,** *47* (20), 7881-7887.

32. Suresh, S. K.; Akkihebbal, K., Anomalous Enhancement of Interphase Transport Rates by Nanoparticles: Effect of Magnetic Iron Oxide on Gas−Liquid Mass Transfer. **2009**.

33. Pang, C.; Lee, J. W.; Kang, Y. T., Review on combined heat and mass transfer characteristics in nanofluids. *International Journal of Thermal Sciences* **2015,** *87*, 49-67.

34. Alper, E.; Wichtendahl, B.; Deckwer, W. D., Gas absorption mechanism in catalytic slurry reactors. *Chemical Engineering Science* **1980,** *35* (1), 217-222.

35. Yoon, S.; Chung, J. T.; Kang, Y. T., The particle hydrodynamic effect on the mass transfer in a buoyant CO2-bubble through the experimental and computational studies. *International Journal of Heat and Mass Transfer* **2014,** *73*, 399-409.

36. Bhattacharya, R. P.; Patrick, E. P. a.; Prajesh, Effect of Aggregation Kinetics on the Thermal Conductivity of Nanoscale Colloidal Solutions (Nanofluid). *Nano Letters* **2006,** *6* (7), 1529-1534.

37. Sadeghinezhad, E.; Mehrali, M.; Saidur, R.; Mehrali, M.; Tahan Latibari, S.; Akhiani, A. R.; Metselaar, H. S. C., A comprehensive review on graphene nanofluids: Recent research, development and applications. *Energy Conversion and Management* **2016,** *111*, 466-487.

38. Yue, S. L.; Rujie, L.; Yining, W.; Fang, H.; Xianren, Z.; Tongtao, Size-, Aggregation-, and Oxidization-Dependent Perturbation of Methane Hydrate by Graphene Nanosheets Revealed by Molecular Dynamics Simulations. *Journal of Physical Chemistry* **2019**.

39. Veilleux, J.; Coulombe, S., A total internal reflection fluorescence microscopy study of mass diffusion enhancement in water-based alumina nanofluids. **2010**.

40. Pasieka, J.; Coulombe, S.; Servio, P., Investigating the effects of hydrophobic and hydrophilic multi-wall carbon nanotubes on methane hydrate growth kinetics. *Chemical Engineering Science* **2013,** *104*, 998-1002.

41. Wen, D.; Lin, G.; Vafaei, S.; Zhang, K., Review of nanofluids for heat transfer applications. *Particuology* **2009,** *7* (2), 141-150.